Neuron
Article

$Ca_V2.3$ Channels Are Critical for Oscillatory Burst Discharges in the Reticular Thalamus and Absence Epilepsy

Tariq Zaman,[1,3] Kyoobin Lee,[1] Cheongdahm Park,[1] Afshin Paydar,[1,3] Jee Hyun Choi,[1,3] Eunji Cheong,[1,3] C. Justin Lee,[1,2,3] and Hee-Sup Shin[1,2,3,*]
[1]Center for Neural Science
[2]Center for Functional Connectomics
Korea Institute of Science and Technology (KIST), Seoul 136-791, Korea
[3]Department of Neuroscience, University of Science and Technology, Daejeon 305-701, Korea
*Correspondence: shin@kist.re.kr
DOI 10.1016/j.neuron.2011.02.042

SUMMARY

Neurons of the reticular thalamus (RT) display oscillatory burst discharges that are believed to be critical for thalamocortical network oscillations related to absence epilepsy. Ca^{2+}-dependent mechanisms underlie such oscillatory discharges. However, involvement of high-voltage activated (HVA) Ca^{2+} channels in this process has been discounted. We examined this issue closely using mice deficient for the HVA $Ca_V2.3$ channels. In brain slices of $Ca_V2.3^{-/-}$, a hyperpolarizing current injection initiated a low-threshold burst of spikes in RT neurons; however, subsequent oscillatory burst discharges were severely suppressed, with a significantly reduced slow afterhyperpolarization (AHP). Consequently, the lack of $Ca_V2.3$ resulted in a marked decrease in the sensitivity of the animal to γ-butyrolactone-induced absence epilepsy. Local blockade of $Ca_V2.3$ channels in the RT mimicked the results of $Ca_V2.3^{-/-}$ mice. These results provide strong evidence that $Ca_V2.3$ channels are critical for oscillatory burst discharges in RT neurons and for the expression of absence epilepsy.

INTRODUCTION

The reticular thalamus (RT) consists of a thin sheet of inhibitory neurons that innervate thalamocortical neurons and modulate rhythmic oscillations in the thalamocortical network. Oscillatory, or rhythmic, activities of the RT are regulated by corticothalamic and thalamocortical synaptic interactions and by reciprocal connections among RT cells (Fuentealba and Steriade, 2005; Huguenard and McCormick, 2007; Steriade, 2006). It has been proposed that the oscillatory activity of the RT can be transferred in a rhythmic fashion to other structures of the thalamocortical network (Steriade et al., 1993). Recently, it was suggested that normal network oscillations provide a template on which seizures driven by neuronal hyperexcitabilities are generated (Beenhakker and Huguenard, 2009). The mechanisms that underlie the network oscillations have been investigated using electroencephalography (EEG) recordings simultaneously with intracellular or extracellular recordings of RT neurons in vivo (Slaght et al., 2002). These studies revealed that oscillatory burst discharges of RT neurons are tightly synchronized and correlated with spike-and-wave discharges (SWDs) observed in EEG, a hallmark of absence seizures. Interestingly, these oscillatory bursts were also observed in isolated RT neurons (Llinas, 1988; Llinas and Steriade, 2006). During oscillatory bursts a burst event is typically followed by slow afterhyperpolarization (AHP), which in turn initiates a next round of burst firings. Slow AHP is recruited by a specific set of Ca^{2+}-dependent mechanisms (Avanzini et al., 1989; Blethyn et al., 2006; Cueni et al., 2008). Recent reports have shown that Ca^{2+} influx through low-voltage activated (LVA) Ca^{2+} channels and subsequent activation of small-conductance Ca^{2+}-activated potassium channels (SKs) during slow AHP are critical for the rhythmic burst discharges of RT cells (Cueni et al., 2008; Pape et al., 2004). The involvement of high-voltage activated (HVA) Ca^{2+} channels in this process has been discounted based on pharmacological data (Cueni et al., 2008).

Among the various types of HVA Ca^{2+} channels, R-type channels ($Ca_V2.3$) are densely expressed in the cortex (Rhee et al., 1999) and RT, but not in the thalamocortical neurons (Weiergraber et al., 2008). $Ca_V2.3$ channels are involved in physiological processes such as neurotransmitter release, synaptic plasticity, fear responses, and nociception (Breustedt et al., 2003; Dietrich et al., 2003; Lee et al., 2002; Saegusa et al., 2000). They also trigger slow AHP in neurons of the suprachiasmatic nuclei (Cloues and Sather, 2003). Functional properties determined by transient expression of $Ca_V2.3$ subunit in *Xenopus laevis* oocytes revealed that although $Ca_V2.3$ channels are structurally related to HVA Ca^{2+} channels, their electrophysiological properties are closer to that of T-type Ca^{2+} channels (Soong et al., 1993), yet their activation threshold is higher than that for T-type channels (Randall and Tsien, 1997). Experimental efforts to define the function of $Ca_V2.3$ channel have been hampered by differential sensitivities of $Ca_V2.3$ splice variants toward the specific blocker, SNX-482 (Tottene et al., 2000).

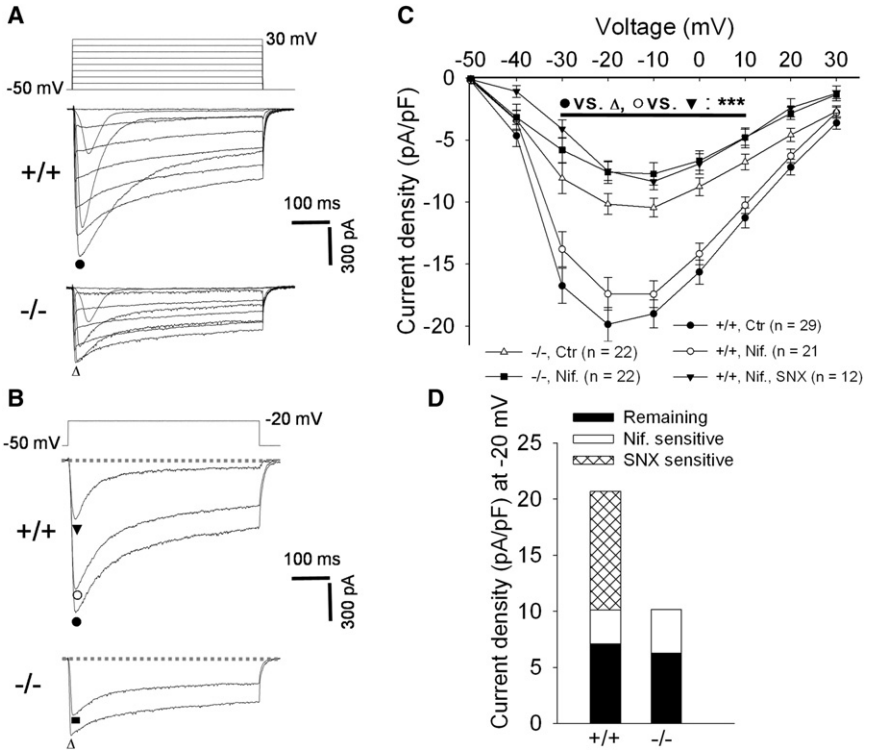

Figure 1. HVA Ca^{2+} Currents Are Significantly Reduced in $Ca_V2.3^{-/-}$ RT Neurons

(A) Representative traces showing HVA Ca^{2+} currents elicited by depolarizing voltage steps from a holding potential of −50 mV to test potentials (500 ms) ranging from −40 to 30 mV in wild-type (top) and $Ca_V2.3^{-/-}$ (bottom) RT neurons.

(B) Traces showing HVA Ca^{2+} currents in wild-type (top) and $Ca_V2.3^{-/-}$ (bottom) neurons under different experimental conditions: control (Ctr); nifedipine (Nif, 10 μM); and SNX-482 (+SNX, 500 nM).

(C) Current-voltage (I–V) curves representing the peak current density of HVA Ca^{2+} currents of $Ca_V2.3^{+/+}$ and $Ca_V2.3^{-/-}$ neurons under different experimental conditions, presented as mean ± SEM (***$p < 0.001$; Student's two-tailed t test).

(D) Bar graph showing the components of HVA Ca^{2+} currents of $Ca_V2.3^{+/+}$ (n = 12) and $Ca_V2.3^{-/-}$ neurons (n = 22) sensitive to different channel blockers: nifedipine or SNX-482.

Mibefradil, which is a potent inhibitor of both $Ca_V2.3$ and T-type channels (Randall and Tsien, 1997), has also not been helpful in defining the role of $Ca_V2.3$ channels. To overcome these limitations we analyzed $Ca_V2.3$-deficient ($Ca_V2.3^{-/-}$) mice, which lack all possible $Ca_V2.3$ splice variants (Lee et al., 2002).

Here, we report that, contrary to the current view, Ca^{2+} influx through $Ca_V2.3$ channels is critical for rhythmic burst discharges of RT neurons. Acute experiments in wild-type slices revealed that a rebound activation of T-type channels recruits $Ca_V2.3$ channels. This sequential channel activation ensures effective recruitment of the Ca^{2+}-dependent slow AHP that is known to be critical for rhythmic burst discharges of RT neurons. Furthermore, the lack of $Ca_V2.3$ channels reduced the susceptibility of mice to absence seizures. This study provides compelling evidence that $Ca_V2.3$ channels are critical for cellular as well as network oscillations that are linked to absence seizures.

RESULTS

$Ca_V2.3$ Channel Currents Are a Major Component of Total HVA Ca^{2+} Current in RT Neurons

The functional loss of $Ca_V2.3$ channels was confirmed electrophysiologically using whole-cell patch clamping of RT neurons in brain slices. HVA-mediated inward currents were evoked by a series of depolarizing voltage steps from a holding potential of −50 mV to test potentials ranging from −40 to +30 mV as described previously (Huguenard and Prince, 1992; Sun et al., 2002). Under these conditions, most LVA Ca^{2+} channels should remain inactivated. The peak current density measured at various test potentials was significantly reduced in RT neurons of $Ca_V2.3^{-/-}$ mice compared with the wild-type ($p < 0.001$; Figures 1A and 1C). To isolate L- and R-type components of HVA Ca^{2+} current, we applied nifedipine, an L-type channel blocker, and SNX-482, an R-type selective blocker (Newcomb et al., 1998, 2000) to wild-type neurons. Compared with $Ca_V2.3^{-/-}$ neurons, a similar reduction in the $Ca_V2.3$ current density was observed in wild-type neurons after adding the SNX-482, even in the presence of nifedipine ($p < 0.001$; Figures 1B and 1C). Comparative analysis of R- and L-type Ca^{2+} currents at −20 mV revealed that a major component of HVA Ca^{2+} currents in RT neurons was sensitive to SNX-482 (50.97% ± 6.45%), a bigger fraction than to nifedipine (18.81% ± 0.68%; $p = 0.001$; Figures 1B and 1D). In this study, nine of 12 cells showed a large reduction (57.91% ± 6.34%), whereas the remaining three cells showed a smaller reduction (26.23% ± 7.6%) in the peak current density, consistent with a previous report that RT cells might harbor different $Ca_V2.3$ splice variants with different SNX-482 sensitivities (Pereverzev et al., 2002). These results suggest that $Ca_V2.3$ channel currents comprise a major component of the total HVA Ca^{2+} current in RT neurons.

LVA Ca^{2+} Currents Are Unaltered in $Ca_V2.3^{-/-}$ RT Neurons

To determine whether the absence of $Ca_V2.3$ affected the LVA Ca^{2+} current density, we measured LVA currents in $Ca_V2.3^{-/-}$ RT neurons using a standard protocol (Huguenard and Prince, 1992; Joksovic et al., 2005). The neurons were typically held at −90 mV (1 s) and depolarized to test potentials ranging from −80 to −50 mV (Sun et al., 2002). This depolarization is below the activation threshold for HVA Ca^{2+} channels and induces a fast-inactivating current, typical of T-type Ca^{2+} currents (Fox et al., 1987). No significant reduction in the peak current density was observed in $Ca_V2.3^{-/-}$ neurons compared to the wild-type

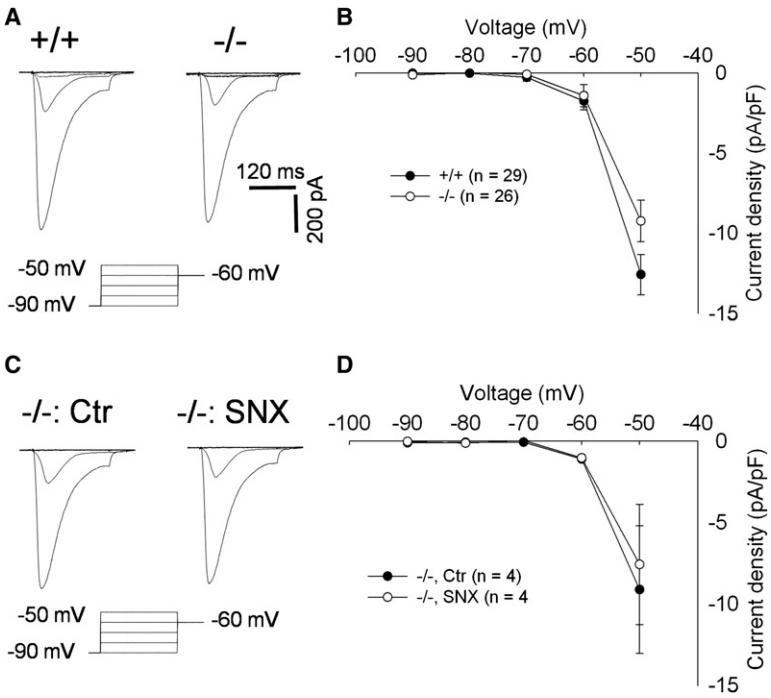

Figure 2. LVA Ca^{2+} Currents Remain Unaltered in $Ca_V2.3^{-/-}$ RT Neurons

(A) Traces showing LVA Ca^{2+} currents elicited in wild-type and $Ca_V2.3^{-/-}$ neurons. LVA Ca^{2+} currents are elicited by depolarizing voltage step (200 ms) from −90 mV to test potentials ranging from −80 to −50 mV.

(B) Peak current density for wild-type (n = 29) and $Ca_V2.3^{-/-}$ (n = 26) neurons. No significant reduction was observed in the peak current density in $Ca_V2.3^{-/-}$ compared with wild-type, presented as mean ± SEM ($^{n.s.}p > 0.05$; Student's two-tailed t test).

(C) To determine whether application of SNX-482 blocks LVA Ca^{2+} channels, inward currents were elicited in the $Ca_V2.3$-deficient RT neurons in the presence or absence of SNX-482 (500 nM). Representative traces showing LVA Ca^{2+} currents in $Ca_V2.3^{-/-}$ RT neurons before and after application of SNX-482 (500 nM).

(D) Peak current density for control and SNX-treated neurons, presented as mean ± SEM ($^{n.s.}p > 0.05$; Student's two-tailed t test). No significant difference was observed before and after the application of SNX-482, consistent with the previous report that SNX-482 selectively blocks $Ca_V2.3$ but not T-type Ca^{2+} channels (Joksovic et al., 2005). $^{n.s.}$, not significant.

at all tested potentials ($p > 0.05$; Figures 2A and 2B). In addition, treatment with 500 nM SNX-482 did not affect the LVA currents in $Ca_V2.3^{-/-}$ RT neurons ($p > 0.05$; Figures 2C and 2D), consistent with a previous report that SNX-482 selectively blocks $Ca_V2.3$ but not T-type Ca^{2+} channels (Joksovic et al., 2005). Taken together, these results indicate that the $Ca_V2.3$ current is selectively impaired by $Ca_V2.3$ knockout or SNX-482 blockade, without affecting LVA Ca^{2+} currents.

Lack of $Ca_V2.3$ Suppresses Oscillatory Burst Discharges in RT Neurons

We next examined the intrinsic firing behaviors of wild-type and $Ca_V2.3^{-/-}$ RT neurons with whole-cell current clamp methods using a K^+-based intracellular solution. Evoked responses were recorded from genetically labeled GFP-positive neurons (Lopez-Bendito et al., 2004) in anatomically distinct regions of dorsal or lateral RT nuclei (Figure 3A) that are known to be associated with visual or motor modalities, respectively (Coleman and Mitrofanis, 1996; Jones, 1975; Lee et al., 2007). Low-threshold (LT) bursting was evoked by a current injection (1 s duration) that ensured a hyperpolarization close to −90 mV. On average −112.89 ± 6.44 pA current was injected, which hyperpolarized the wild-type cells by −31.86 ± 0.66 mV from the initial baseline potential of −60 mV. Similarly, a −118.84 ± 8.97 pA current injection hyperpolarized the $Ca_V2.3^{-/-}$ neurons by −29.35 ± 1.14 mV from the initial baseline potential of −60 mV. We found that similar percentages of RT neurons in both dorsal and lateral regions of wild-type mice showed rhythmic burst discharges or single-burst firing only (Figure 3B; see Table S1 available online). Approximately 60% of wild-type neurons (n = 40) showed rhythmic burst discharges, with 2–13 burst discharges, each typically containing 2–8 action potentials at 209.47 ± 9.69 Hz; about 25% (n = 17) showed only a single LT burst, and 15% (n = 10) exhibited no LT burst at all (Figures 3B and 3C; Table S1).

Next, we examined $Ca_V2.3^{-/-}$ neurons in a similar manner. The most conspicuous finding was a dramatic suppression of rhythmic burst discharges in the majority of $Ca_V2.3^{-/-}$ neurons; only 10% (5 of 49) exhibited rhythmic burst discharges, whereas 67% (33 of 49) exhibited a single LT burst, and 23% (11 of 49) showed no LT burst at all (Figures 3B and 3C; Table S1). The onset of LT burst, assessed by comparing the time points between end of hyperpolarization and the first action potential, was significantly delayed in $Ca_V2.3^{-/-}$ neurons (205.74 ± 24.55 ms) compared to wild-type neurons (134.58 ± 9.12 ms; p = 0.002). The total number of burst events was also significantly reduced in $Ca_V2.3^{-/-}$ neurons (1.16 ± 0.08) compared to wild-type neurons (6.16 ± 0.55; p = 0.0001; Figure 3D), as were the number of spikes in a burst (3.16 ± 0.31 in $Ca_V2.3^{-/-}$ versus 4.77 ± 0.30 in wild-type; p = 0.001; Figure 3E) and the intraburst spike frequency (126.67 ± 10.38 Hz in $Ca_V2.3^{-/-}$ versus 209.47 ± 9.69 Hz in wild-type, p = 0.0003). On the other hand, the characteristic accelerating-decelerating pattern of intraburst spikes (Llinas and Steriade, 2006; Steriade et al., 1986) remained unchanged in the mutant in the majority of neurons tested (Figure S1A). Notably, the amplitude of slow AHP following the initial LT burst was significantly reduced in $Ca_V2.3^{-/-}$ neurons (−3.59 ± 0.65 mV) compared to that in wild-type neurons (−10.96 ± 0.48 mV; p = 0.0004; Figure 3F). We found that the amplitude of slow AHP was positively correlated with the number and the frequency of intraburst spikes (Pearson correlation coefficient: 0.731 and 0.727, respectively) of the first LT burst (Figures S1B and S1C).

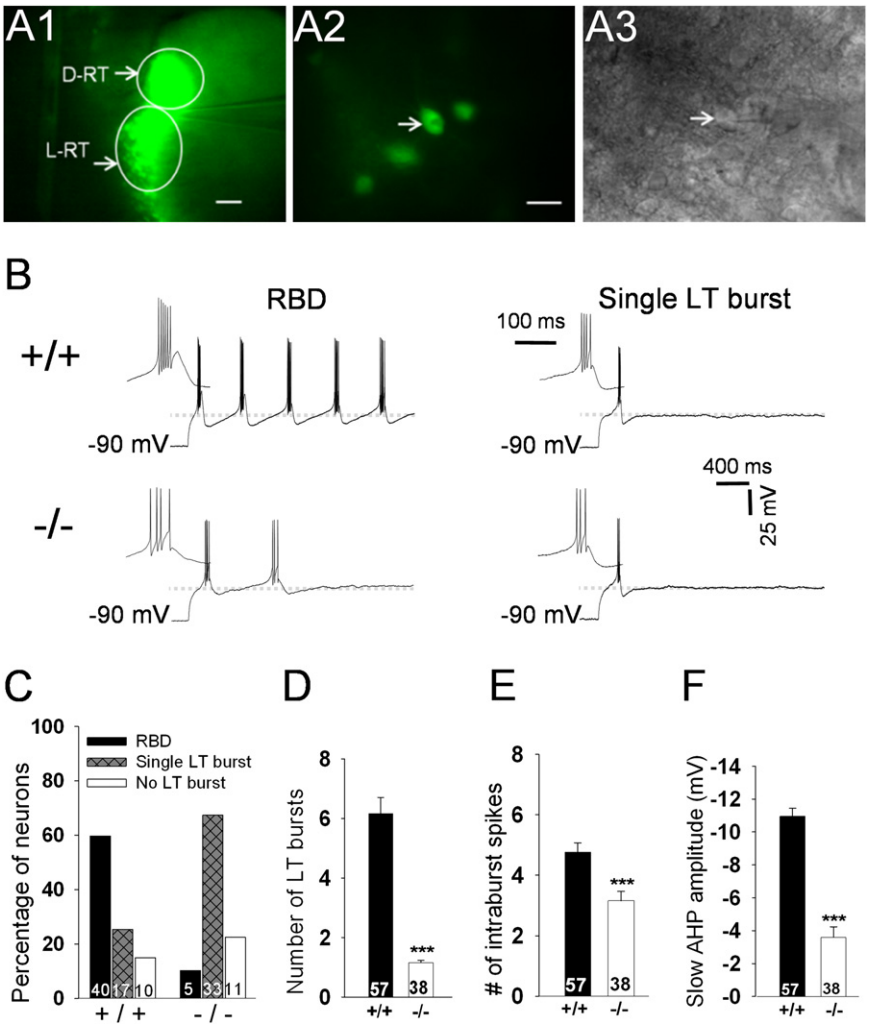

Figure 3. The Lack of $Ca_V2.3$ Channels in RT Neurons Suppresses Rhythmic Burst Discharges and Reduces Slow AHP

(A1–A3) Image from recording chamber (A1) showing regions studied (D-RT, dorsal RT; L-RT, lateral RT) with (A2) GFP and (A3) differential interference contrast (DIC) images of the patched neuron. Evoked responses were recorded from GFP-labeled neurons. Scale bars in (A1) and (A2) represent 0.2 mm and 20 μm, respectively.

(B) Representative traces showing rhythmic burst discharges (RBD, left panel) or a single LT burst (right panel) in wild-type (upper traces) and $Ca_V2.3^{-/-}$ (lower traces) RT neurons. For a clearer view, the first LT burst is expanded. Dotted lines correspond to the holding potential of −60 mV.

(C) Bar graph showing the intrinsic firing pattern (RBD, a single LT burst, or no LT burst) in terms of percentage in wild-type versus $Ca_V2.3^{-/-}$ neurons. The majority of $Ca_V2.3^{-/-}$ neurons showed a marked suppression of rhythmic burst discharges compared with wild-type.

(D) Bar graph showing the total number of LT burst discharges in wild-type (n = 57) and $Ca_V2.3^{-/-}$ neurons (n = 38), presented as mean ± SEM (***$p < 0.001$; Student's two-tailed t test).

(E) Quantitative analysis of intraburst spikes in the initial LT burst between wild-type and $Ca_V2.3^{-/-}$ neurons, presented as mean ± SEM (***$p < 0.001$; Student's two-tailed t test).

(F) Comparison of the amplitude of LT burst-induced slow AHP in wild-type and $Ca_V2.3^{-/-}$ neurons. Slow AHP amplitude was measured from the threshold potential of the first spike within the first LT burst to the peak of the hyperpolarizing voltage deflection that follows the burst. The number on each bar represents the number of neurons tested. All data are presented as mean ± SEM (***$p < 0.001$).

To examine whether rhythmic burst discharges are influenced by synaptic activities, we carried out control experiments in synaptically isolated neurons. Treatment with both picrotoxin (50 μM) and kynurenic acid (4 mM) did not affect the total number of burst events (11.8 ± 3.49 in the $Ca_V2.3^{+/+}$ control versus 9.75 ± 3.21 in picrotoxin/kynurenic acid-treated $Ca_V2.3^{+/+}$, n = 5; p = 0.678; Figures S1D–S1F). These results suggest that the effect of $Ca_V2.3$ deletion on the rhythmic burst discharge was largely based on its effect on the intrinsic property of RT neurons.

Interestingly, neurons from $Ca_V2.3^{+/-}$ heterozygote mice showed firing-pattern and spike-frequency values intermediate between those of wild-type and homozygous $Ca_V2.3^{-/-}$ mice (Figures S1G and S1H). There were no significant differences in the membrane properties (Table S1), or amplitudes and half-widths of action potentials between wild-type and $Ca_V2.3^{-/-}$ neurons (data not shown).

Taken together, these results suggest that Ca^{2+} influx through $Ca_V2.3$ channels contributes substantially to the strength of LT bursts and the recruitment of slow AHPs, which are critical for rhythmic burst discharges of RT neurons.

Pharmacological Dissection Confirms a Contribution of $Ca_V2.3$ Currents to Cellular Oscillation

To examine whether pharmacological inactivation of $Ca_V2.3$ channels can mimic the effect of the mutation on the firing pattern, first we treated three wild-type neurons with 100 nM of $Ca_V2.3$ channel blocker, SNX-482, as was used in the report (Cueni et al., 2008). This concentration was ineffective in mimicking the mutant results. However, the application of 500 nM SNX-482 almost completely eliminated rhythmic burst discharges in wild-type RT neurons, leaving only a single LT burst (6.4 ± 1.29 burst discharges in control versus 1.04 ± 0.04, with SNX, n = 5 each; p = 0.003; Figures 4A and 4C), faithfully phenocopying the $Ca_V2.3$ knockout. The onset of LT burst was delayed in SNX-482 treated $Ca_V2.3^{+/+}$ neurons (192.40 ± 19.15 ms) compared with $Ca_V2.3^{+/+}$ control (138.2 ± 8.96; p = 0.033), with a significant reduction in the number of intraburst spikes (4.6 ± 0.24 in SNX-482 treated $Ca_V2.3^{+/+}$ neurons versus 5.8 ± 0.37 in control; p = 0.028; Figures 4A and 4D) and the frequency (178.11 ± 22.14 Hz in SNX-482 treated $Ca_V2.3^{+/+}$ neurons versus 236.80 ± 10.16 Hz in $Ca_V2.3^{+/+}$ control; p = 0.042). Moreover, the amplitude of slow AHP following the

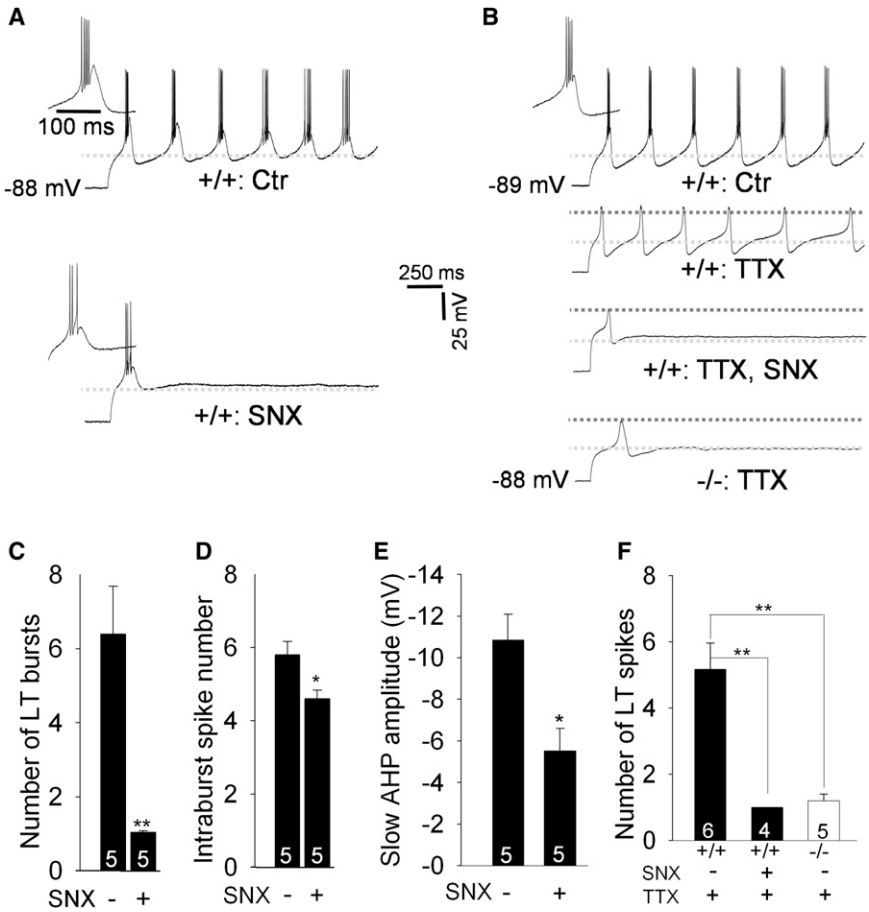

Figure 4. Pharmacological Dissection of Rhythmic Discharges in RT Neurons Confirms the Contribution of $Ca_V2.3$ Currents to the Recruitment of Slow AHP

(A) Traces showing responses in a wild-type neuron before (top) and after (middle trace) the application of SNX-482 (500 nM; n = 5). Hyperpolarization is induced by negative current injection (120–150 pA). For a clearer view, the first LT burst is expanded.

(B) Traces showing discharge patterns of Ca^{2+} spikes in the presence of TTX (500 nM). Top shows traces from wild-type RT neurons before (first trace) and after (second trace) the application of TTX; third trace after the application of SNX-482 (+SNX, 500 nM); fourth trace represents $Ca_V2.3^{-/-}$. Ctr, control; SNX, SNX-482; dark and light-gray dotted lines correspond to −30 and −60 mV, respectively.

(C and D) Bar graph showing the number of LT burst discharges and the number of intraburst spikes in wild-type RT neurons before and after SNX-482 application.

(E) Slow AHP amplitude in the wild-type before and after application of SNX-482.

(F) Bar graph showing the total number of Ca^{2+} spikes in the presence of TTX (500 nM) in wild-type, $Ca_V2.3^{-/-}$, and SNX-482-treated RT neurons. All data are presented as mean ± SEM. The number on each bar represents the neurons examined (**p < 0.01).

initial LT burst was greatly reduced in the presence of SNX-482 (−10.86 ± 1.23 mV in control versus −5.52 ± 1.09 mV with SNX, n = 5 each; p = 0.012; Figures 4A and 4E), similar to the results observed in $Ca_V2.3^{-/-}$ neurons (Figure 3F).

Next, to examine in detail whether an initial low-threshold Ca^{2+} spike (LTS) can activate slow AHP and subsequent oscillatory discharges, we isolated Ca^{2+} spikes by blocking fast sodium spikes using the Na^+ channel blocker, tetrodotoxin (TTX; 500 nM). In the presence of TTX, the first Ca^{2+} spike was intact, but rhythmic Ca^{2+} spikes were markedly suppressed in $Ca_V2.3^{-/-}$ neurons (1.2 ± 0.20, n = 5) compared with wild-type neurons (5.17 ± 0.79, n = 6; p = 0.002; Figures 4B and 4F). Application of SNX-482 (500 nM) to wild-type neurons similarly suppressed rhythmic Ca^{2+} spikes (5.17 ± 0.79 in control [n = 6] versus 1 ± 0.00 for SNX [n = 4]; p = 0.003; Figures 4B and 4F), leaving only the first spike intact. The time to the LTS peak was significantly increased in SNX-482 treated $Ca_V2.3^{+/+}$ (282.25 ± 38.78 ms; p = 0.004) and $Ca_V2.3^{-/-}$ neurons (275.40 ± 20.53 ms; p = 0.001) compared with $Ca_V2.3^{+/+}$ (142.50 ± 12.17 ms). The amplitude of LTS measured from the first inflection to the peak was reduced in SNX-482 treated $Ca_V2.3^{+/+}$ (22.83 ± 1.37 mV; p = 0.02) and $Ca_V2.3^{-/-}$ neurons (21.84 ± 1.13 mV; p = 0.006) compared with $Ca_V2.3^{+/+}$ (27.97 ± 1.22 mV), suggesting the role of $Ca_V2.3$ in generating depolarization following the activation of T-currents. The width of LTS, measured between the points of inflection to deflection, was prolonged in $Ca_V2.3^{-/-}$ neurons (219.75 ± 35.69 ms; p = 0.013) as well as SNX-482 treated $Ca_V2.3^{+/+}$ (185.6 ± 21.78 ms; p = 0.037) compared with the wild-type (135.01 ± 6.92 ms), suggesting an inefficient activation of Ca^{2+}-dependent slow AHP. These results support the idea that $Ca_V2.3$ channels contribute to the strength of the Ca^{2+} spike that is critical for the recruitment of slow AHP.

Slow AHP is induced by selective coupling of voltage-insensitive SK_2 channels with distinct sets of Ca^{2+} channels. To examine the involvement of SK_2 channels in slow AHP in this system (Debarbieux et al., 1998), we isolated SK_2 currents by utilizing the SK_2-specific blocker, apamin, a bee-venom toxin (Sah, 1996; Sah and McLachlan, 1991). Sample traces are shown in Figure 5A. Before adding apamin, currents evoked by depolarizing steps (50 ms) from −60 mV to −30, −20, or −10 mV were 0.32 ± 0.14, 0.48 ± 0.12, and 0.69 ± 0.13 $pApF^{-1}$ in $Ca_V2.3^{-/-}$ neurons (n = 9), respectively, compared to the corresponding values of 1.11 ± 0.14, 1.64 ± 0.15, and 1.96 ± 0.13 $pApF^{-1}$ (n = 11) in wild-type RT neurons (p < 0.001; Figure 5B). These results suggest that SK_2 currents were significantly reduced in $Ca_V2.3^{-/-}$ neurons compared to the wild-type.

Next, to examine the amplitude of SK_2 currents under the conditions close to that of LT bursting, the currents were

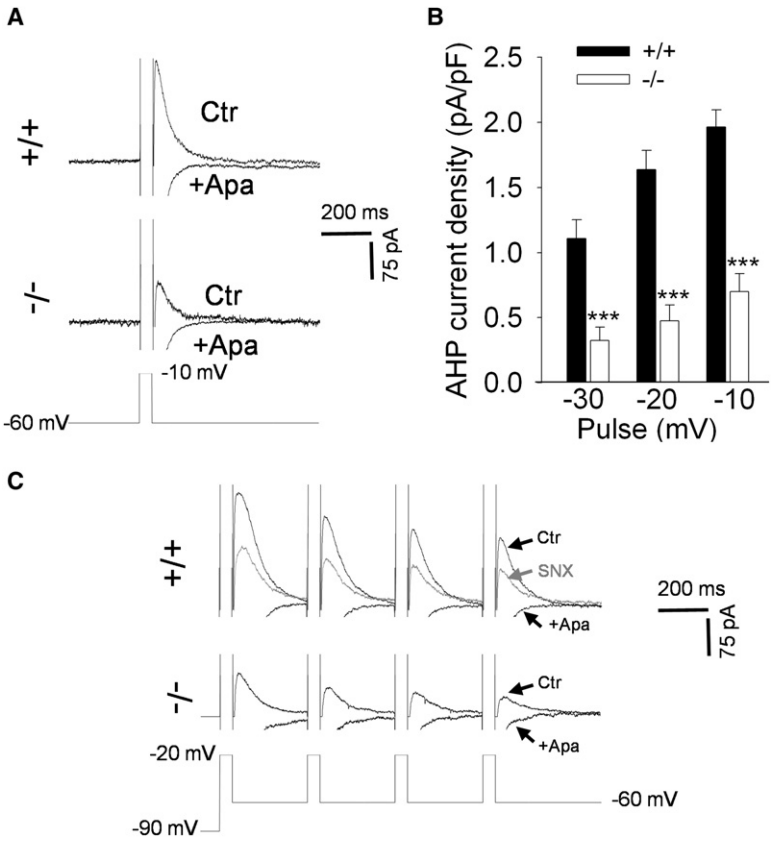

Figure 5. $Ca_V2.3$ Channels in RT Neurons Are Critical for SK_2 Currents

(A) Representative traces showing K^+-based AHP currents (Ctr) that were completely reduced after the application of 100 nM apamin (+Apa) in $Ca_V2.3^{+/+}$ and $Ca_V2.3^{-/-}$ RT neurons. Bottom shows voltage steps from −60 to −10 mV (50 ms).

(B) Quantitative analysis of the AHP current density in $Ca_V2.3^{+/+}$ (n = 11) and $Ca_V2.3^{-/-}$ (n = 9) RT neurons, evoked by different depolarizing steps (50 ms) from −60 mV to −30, −20, and −10 mV, presented as mean ± SEM (***p < 0.01; Student's two-tailed t test).

(C) Traces showing AHP currents activated by repeated voltage gating of Ca^{2+} channels at −20 mV in $Ca_V2.3^{+/+}$ neurons (n = 3) before (Ctr) and after (SNX) the application of 500 nM SNX-482. For the comparison these currents were evoked in $Ca_V2.3^{-/-}$ neurons (n = 3). A subsequent application of 100 nM apamin (+Apa) to both experimental groups completely blocked the AHP currents.

activated by repeated voltage gating of Ca^{2+} channels (Cueni et al., 2008) at −20 mV. Compared with the wild-type control (2.61 ± 0.11, 1.71 ± 0.13, 1.3 ± 0.07, and 0.97 ± 0.05 $pApF^{-1}$), SK_2 currents were smaller in SNX-482 treated $Ca_V2.3^{+/+}$ neurons (1.19 ± 0.13, 0.87 ± 0.04, 0.79 ± 0.03, and 0.69 ± 0.04 $pApF^{-1}$) but were comparable to those of $Ca_V2.3^{-/-}$ neurons (1.08 ± 0.13, 0.64 ± 0.04, 0.57 ± 0.02, and 0.51 ± 0.01 $pApF^{-1}$; Figure 5C). These results suggest that the insufficient Ca^{2+} influx in $Ca_V2.3^{-/-}$ and SNX-482 treated $Ca_V2.3^{+/+}$ neurons lead to smaller SK_2 currents and, thus, smaller slow AHP. In summary the results from both $Ca_V2.3^{-/-}$ neurons and SNX-482-treated wild-type RT neurons suggest that the Ca^{2+} spike mediated by the T-type channel recruits $Ca_V2.3$ channels to further enhance the Ca^{2+} influx, which then successfully recruits slow AHP, leading to the next round of T-type channels activation, perpetuating rhythmic burst discharges.

$Ca_V2.3$ Channels Enhance the Tonic Firing Activity of RT Neurons

It was demonstrated previously that a blockade of slow AHP by apamin induced a hyperexcitability in the neurons of RT (Debarbieux et al., 1998). Consistent with this report, we observed a shortening of the period of the apamin-induced hyperexcitability in $Ca_V2.3^{-/-}$ neurons (Figure S2A, middle traces, and Figure S2B). Furthermore, in the presence of TTX, apamin blocked rhythmic discharges of Ca^{2+} spikes and induced a depolarization in the membrane potential of wild-type RT neurons, unmasking a slowly decaying plateau potential (Figure S2A, bottom traces); these results are consistent with previous reports (Cueni et al., 2008; Yazdi et al., 2007). When compared at the midpoint of the response, the plateau potential was significantly more negative in $Ca_V2.3^{-/-}$ neurons (−44.23 ± 1.65 mV, n = 9) than that in wild-type neurons (−34.23 ± 2.01 mV, n = 5; p = 0.002), suggesting a contribution of $Ca_V2.3$ channels to this membrane depolarization.

A small depolarization from the resting membrane potential increases the excitability of thalamic neurons (Llinas, 1988; Perez-Reyes, 2003). The reduced plateau potential in $Ca_V2.3^{-/-}$ neurons indicates a possible role of $Ca_V2.3$ channels in the membrane depolarization following an activation of T-currents. To examine this possibility, depolarizing currents (10 pA increments; eight steps; 1 s duration) were injected from a holding potential of −60 mV, close to the resting membrane potential (−61.96 ± 0.63 mV in $Ca_V2.3^{+/+}$ versus −62.52 ± 0.65 mV in $Ca_V2.3^{-/-}$). In response to depolarizing inputs (10–80 pA), RT neurons fired an initial high-frequency burst followed by low-frequency tonic spikes. The number of intraburst spikes was significantly reduced in $Ca_V2.3^{-/-}$ neurons (2.01 ± 0.41 to 3.85 ± 0.26, n = 13 of 38) compared with the wild-type (4.83 ± 0.36 to 6.84 ± 0.27, in $Ca_V2.3^{+/+}$, n = 36 of 57; p = 0.0001; Figures 6A and 6B). Similarly, subsequent tonic spike frequencies at 10–80 pA current injections were significantly reduced in $Ca_V2.3^{-/-}$ neurons (2.5 ± 0.29 to 26.61 ± 1.38 Hz, n = 38) compared with $Ca_V2.3^{+/+}$ (3.79 ± 0.38 to 39.38 ± 1.11 Hz, n = 57; p = 0.015 to 0.0002; Figures 6A and 6C). These results show that $Ca_V2.3$ channels enhance the tonic firing activity of RT neurons.

Lack of $Ca_V2.3$ Channels Reduces Susceptibility to Absence Seizures in Mice

Intracellular recordings during SWDs have revealed that high-frequency rhythmic bursts of RT neurons are tightly synchronized

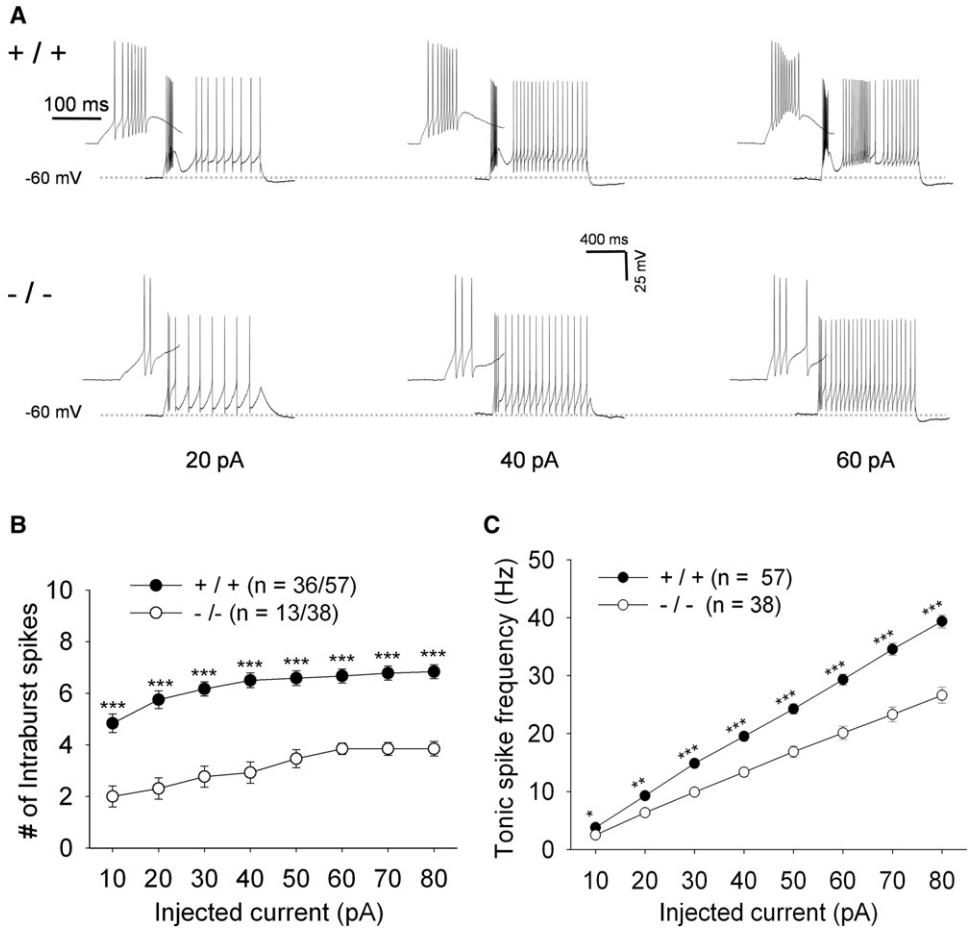

Figure 6. $Ca_V2.3$ Channels Contribute to Tonic Firing Activity of RT Neurons

(A) Representative traces showing responses to 20, 40, and 60 pA of depolarizing currents, in wild-type (top) and $Ca_V2.3^{-/-}$ neurons (bottom), initially held at −60 mV. Input resistance of both groups statistically was not different. For a clearer view, the first LT burst is expanded.

(B) Line graph showing the number of intraburst spikes (during 1 s test pulse), presented as mean ± SEM (***p < 0.001; Student's two-tailed t test).

(C) Quantitative analysis of the tonic spike frequency in response to various depolarizing currents, presented as mean ± SEM (*p < 0.05, **p < 0.01, ***p < 0.001; Student's two-tailed t test).

and correlated with SWDs (Slaght et al., 2002). To examine the physiological consequences of the $Ca_V2.3$ deficiency, we examined the susceptibility of $Ca_V2.3^{-/-}$ mice to drug-induced absence seizures. SWDs were induced by systemic administration of gamma-butyrolactone (GBL), a prodrug of γ-hydroxy butyrate (Ishige et al., 1996; Snead, 1988), and seizure activities were monitored by recording epidural EEGs. Both monopolar and bipolar EEG recordings were performed in parallel on each mouse to allow comparisons with previously reported bipolar EEG recordings from similar mutant mice (Weiergraber et al., 2008). Administration of GBL (70 mg/kg body weight, i.p.) to $Ca_V2.3^{+/+}$ (n = 12), $Ca_V2.3^{+/-}$ (n = 5), and $Ca_V2.3^{-/-}$ mice (n = 16) at the age of ~16 weeks induced typical paroxysmal SWDs in all genotypes. However, the severity of the SWD response was reduced in $Ca_V2.3^{-/-}$ mice compared with $Ca_V2.3^{+/+}$ animals (Figure 7A), as reflected in the decrease in the duration of SWDs during each time segment ($F(1, 26) = 331.647$; $p < 0.001$, two-way repeated ANOVA; Figure 7B). The total SWD duration during the 30 min observation period was also significantly reduced in $Ca_V2.3^{-/-}$ mice (309.81 ± 17.78 s) compared with $Ca_V2.3^{+/+}$ mice (820.40 ± 22.08 s; $p < 0.001$; Figure 7D), as was the mean duration of each SWD event (2.83 ± 0.04 s in $Ca_V2.3^{-/-}$ versus 4.85 ± 0.01 s in $Ca_V2.3^{+/+}$; $p < 0.001$; Figure 7E). The time-to-onset of SWDs was not significantly altered in $Ca_V2.3^{-/-}$ mice, although there was a tendency toward a delay in these animals (160.15 ± 6.68 s in $Ca_V2.3^{-/-}$ versus 125.66 ± 9.23 s in $Ca_V2.3^{+/+}$; $p = 0.31$; Figure 7C). Interestingly, $Ca_V2.3^{+/-}$ heterozygous mice showed a level of SWD response intermediate between that of $Ca_V2.3^{-/-}$ and $Ca_V2.3^{+/+}$, indicating a gene dosage effect. A power spectrum density analysis showed that the 3 Hz frequency was dominant during the SWD responses, and the power was stronger in $Ca_V2.3^{+/+}$ mice than in $Ca_V2.3^{-/-}$ during the 20 min following the GBL injection (Figures S3A and S3D).

We have also confirmed the reduced sensitivity of the mutant mice to GBL-induced SWDs at the ages (3 weeks old) similar to

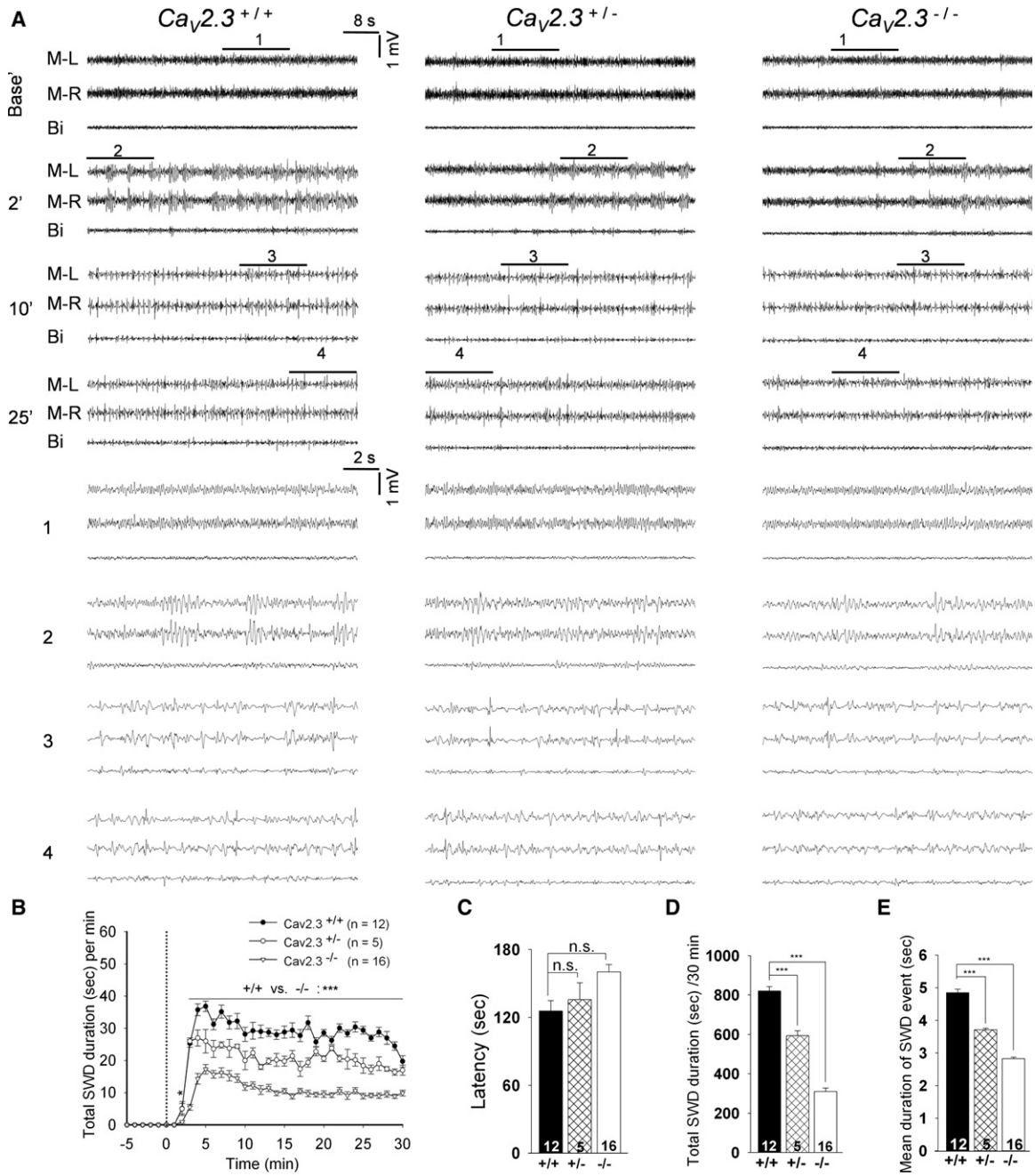

Figure 7. The Strength of GBL-Induced SWDs Is Significantly Reduced in $Ca_V2.3^{-/-}$ Mice

(A) In the upper half, representative traces for real-time monopolar and bipolar EEG recordings from $Ca_V2.3^{+/+}$ (n = 12), $Ca_V2.3^{+/-}$ (n = 5), and $Ca_V2.3^{-/-}$ (n = 16) mice are illustrated according to time (1 min each per line). M-L, monopolar left hemisphere; M-R, monopolar right hemisphere; Bi, bipolar EEG traces. Base represents baseline, and 2′, 10′, and 25′ represent each time point (minutes) after the administration of GBL (70 mg/kg, i.p.). The portions marked by horizontal bars in upper traces (labeled 1–4) are illustrated on an expanded time scale (15 s) below.

(B) Quantification of total SWD duration per 1 min bin before and after the drug injection. The vertical dotted line indicates the time of the drug injection. The horizontal solid line indicates the area showing a p value <0.001 in a two-way ANOVA for the mutant and the wild-type.

(C) Quantitative analysis of the latency to the beginning of SWDs. The onset time of SWDs was not significantly altered in $Ca_V2.3^{-/-}$ mice compared with the wild-type, presented as mean ± SEM ($^{n.s.}p > 0.05$; Student's two-tailed t test).

(D) Total duration of each SWD during the 30 min of observation after the administration of GBL, presented as mean ± SEM (***p < 0.001; Student's two-tailed t test).

(E) Mean duration of each SWD event induced by GBL in $Ca_V2.3^{+/+}$, $Ca_V2.3^{+/-}$, and $Ca_V2.3^{-/-}$ mice, presented as mean ± SEM (***p < 0.001; Student's two-tailed t test). $^{n.s.}$, not significant.

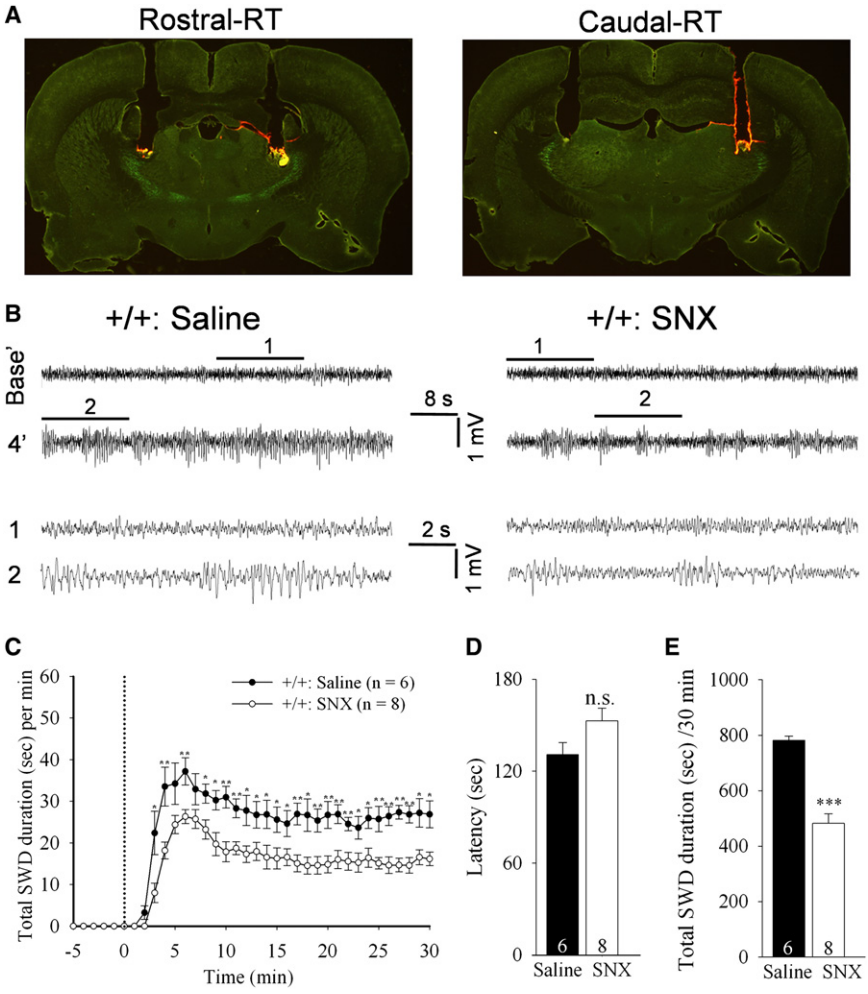

Figure 8. The RT-Specific Blocking of $Ca_V2.3$ in Wild-type Mice Reduces GBL-Induced SWDs

(A) Representative images showing positions of bilateral cannula placements in the rostral (left) and caudal RT (right).

(B) Monopolar EEG traces (1 min each) representing the saline (n = 6) and the SNX-482 injected control mice (n = 8) at the age of 12–16 weeks. Base represents the baseline EEG (25 min after the SNX-482 injection), and 4′ represents time point (minutes) after the administration of GBL (70 mg/kg, i.p.). The portions marked by 1 and 2 are illustrated on an expanded time scale (15 s) below.

(C) Total duration of SWDs (in seconds) per minute before and after the GBL drug administration, presented as mean ± SEM (*$p < 0.05$, **$p < 0.01$; Student's two-tailed t test).

(D) A comparison of the latency to the beginning of SWDs, presented as mean ± SEM ($^{n.s.}p > 0.05$; Student's two-tailed t test).

(E) Total duration of GBL-induced SWDs during the 30 min observation period, presented as mean ± SEM (***$p < 0.001$; Student's two-tailed t test). $^{n.s.}$, not significant.

that of the mice used for patch-clamping recordings, as shown in Figure S4.

Local Blockade of $Ca_V2.3$ Channels in the RT Mimics the Results of Mutant Mice

To examine whether the reduced sensitivity of the mutant mice toward GBL-induced SWDs specifically resulted from the $Ca_V2.3$ deficiency at the RT, we injected SNX-482 bilaterally into the rostral and caudal RT of wild-type mice (Figure 8A) and examined the susceptibility of these injected mice to GBL-induced SWDs. We found a marked reduction in the power and duration of SWDs in SNX-injected mice (n = 8) compared with saline-injected control (n = 6) at the age of 12–16 weeks (Figure 8B). Analysis also showed that the duration of SWD in each time segment was significantly reduced in the SNX-treated group compared with the saline control group (Figure 8C). A tendency toward a delay in the onset of SWDs, although statistically insignificant, was observed in the SNX group (152.91 ± 8.07 s in SNX versus 130.83 ± 7.96 s in saline; $p = 0.81$; Figure 8D). The total SWD duration during the 30 min observation period was also significantly reduced in the SNX group (482.38 ± 34.31 s) compared with the saline group (781.85 ± 15.66 s; $p < 0.0007$; Figure 8E), as was the mean SWD duration (2.25 ± 0.08 s in the SNX group versus 4.55 ± 0.28 s in the saline group; $p < 0.001$).

A power spectrum density analysis of EEG in control animals showed that the GBL-induced SWDs predominate in the 3–4 Hz frequency range, as shown previously (Hu et al., 2001; Kim et al., 2001; Snead, 1988). We found a significant reduction in the power of EEG at the 3–4 Hz frequency in SNX-482 injected mice during the 30 min following the GBL injection (data not shown).

These results indicate that the lack of the $Ca_V2.3$ channel activity in the RT reduces the susceptibility of the mouse to GBL-induced SWDs, suggesting a role for $Ca_V2.3$ channels in the RT in the genesis of SWDs, one of the characteristics of absence seizures.

DISCUSSION

Here, we have demonstrated that $Ca_V2.3$ channels are critical for rhythmic burst discharges of RT neurons and for normal expression of GBL-induced SWDs. We found that although the first LT burst was initiated in $Ca_V2.3^{-/-}$ RT neurons, there was a reduction in the number and frequency of intraburst spikes in the burst, and subsequent rhythmic burst discharges were severely suppressed. Consequently, mice deficient for $Ca_V2.3$ channels showed a reduced susceptibility to GBL-induced SWD responses, one of the key features of absence seizures.

Contribution of $Ca_V2.3$ Channels to HVA Ca^{2+} Currents in RT Neurons

L-, N-, P/Q-, and R-type HVA Ca^{2+} channels are expressed in RT neurons (Huguenard and Prince, 1992; Weiergraber et al., 2008). N- and P/Q-types have been shown to be specifically involved in supporting synaptic transmission (Takahashi and Momiyama, 1993). A substantial proportion of Ca^{2+} currents in the RT is sensitive to Ni^{2+} (Huguenard and Prince, 1992; Joksovic et al., 2009), which blocks both $Ca_V2.3$ (Zamponi et al., 1996) and T-type channels (Joksovic et al., 2005). The characteristics of the $Ca_V2.3$ component of Ca^{2+} currents have remained elusive because it is also potently inhibited by the T-type blocker, mibefradil (Randall and Tsien, 1997), and because different $Ca_V2.3$ splice variants are differentially sensitive to the $Ca_V2.3$ channel blocker, SNX-482 (Tottene et al., 2000). In this latter context some of the numerous splice variants of $Ca_V2.3$ transcripts (Pereverzev et al., 2002) skip exons in the domain II-III (Weiergraber et al., 2006) and, thus, could yield a wide spectrum of outcomes, given that SNX-482 interacts specifically with the domain III and IV (Bourinet et al., 2001). Our results of $Ca_V2.3^{-/-}$ mice, which lack all possible $Ca_V2.3$ splice variants (Lee et al., 2002), demonstrated that a substantial portion of the total HVA Ca^{2+} current was deleted in $Ca_V2.3^{-/-}$ RT neurons, whereas LVA currents were not changed. In our study, 51% of HVA currents were found sensitive to SNX-482, 19%, to nifedipine, and the remaining 30% were insensitive to both. The percentage of nifedipine-sensitive HVA currents in this study was similar to that obtained with nimodipine, as reported previously (Huguenard and Prince, 1992). These results suggest that the $Ca_V2.3$ channels contribute a major portion to HVA Ca^{2+} currents in RT neurons.

Contribution of $Ca_V2.3$ Channels to the Recruitment of Slow AHP

Under the current clamp conditions, releasing a hyperpolarizing pulse in RT neurons recruits a specific set of Ca^{2+}-dependent mechanisms that generates rhythmic burst discharges. It is known that the Ca^{2+}-dependent slow AHP is permissive for repetitive burst generation by allowing T-type channels to recover from inactivation (Bourinet et al., 2001; Cueni et al., 2008; Pape et al., 2004). To our knowledge, the involvement of $Ca_V2.3$ channels in slow AHP has not been clearly demonstrated in RT neurons until now. In fact this possibility was largely discounted based on pharmacological experiments (Cueni et al., 2008). The contribution of $Ca_V2.3$ channels to slow AHP was previously proposed based on experimental results in neurons of the suprachiasmatic nuclei of the rat (Cloues and Sather, 2003), although conclusive evidence was lacking because the experiments were conducted in the presence of Ni^{2+}, which blocks both $Ca_V2.3$ and T-type channels.

Our current- and voltage-clamp studies in brain slices in which R-type channels were genetically ablated or pharmacologically abolished provide compelling evidence that R-type channels contribute to the recruitment of slow AHP in neurons of the RT. In addition, LVA Ca^{2+} currents in $Ca_V2.3^{-/-}$ neurons remained unchanged compared to wild-type neurons, and were unaffected by 500 nM SNX-482, confirming a previous report that SNX-482 specifically blocks $Ca_V2.3$ channels (Joksovic et al., 2005), and supporting the idea that the effect of the $Ca_V2.3^{-/-}$ ablation or SNX-482 treatment on slow AHP was not due to a change in T-type channels under those conditions.

$Ca_V2.3$ Channels and Oscillatory Burst Discharges

It is known that oscillatory burst discharges are an intrinsic property of RT neurons (Debarbieux et al., 1998; Llinas, 1988; Llinas and Steriade, 2006). The involvement of $Ca_V2.3$ channels in the modulation of intrinsic firing patterns was suggested based on their similarity to T-type channels in electrophysiological properties (Soong et al., 1993). Here, our results obtained from experiments using genetics and pharmacology demonstrated that $Ca_V2.3$ channels are critical for the oscillatory burst discharges in RT neurons.

Our results suggest that Ca^{2+} influx mediated by T-type channels alone is not sufficient to maintain the elevated Ca^{2+} level required for the induction of slow AHP, which prepares the cell to fire the next round of LT burst discharges. It has been reported that an increase in the Ca^{2+} level in mossy fibers in the hippocampus facilitates the $Ca_V2.3$ channel activity (Brenowitz and Regehr, 2003). These Ca^{2+}-induced Ca^{2+} responses are severely impaired in HEK293 cells exogenously expressing a $Ca_V2.3$ subunit in which the II-III loop was deleted (Leroy et al., 2003). Similarly, it is possible that the Ca^{2+} influx through T-type channels in RT neurons not only induces depolarization leading to the activation of but may also facilitate the Ca^{2+}-sensitive activity of $Ca_V2.3$ channels. Therefore, we may propose that $Ca_V2.3$ channels, in addition to other players, including T-type Ca^{2+} channels, the SR-ER Ca^{2+} ATPase (SERCA), and SKs (Cueni et al., 2008; Huguenard, 1996; Llinas, 1988; Perez-Reyes, 2003), have a critical role in oscillatory burst discharges in RT neurons.

Simulation of such oscillatory discharges in a model neuron further strengthens our proposal: a simulated neuron lacking $Ca_V2.3$ component of Ca^{2+} currents mimics very closely the firing pattern of the mutant neurons in the experimental setting (Figure S5). For details on simulation see Supplemental Experimental Procedures.

Contribution of $Ca_V2.3$ Channels to the Excitability of RT Neurons

$Ca_V2.3$ channels appear to play an important role in boosting the excitability of RT neurons. A significant reduction in the number of intraburst spikes in the first LT burst was observed in $Ca_V2.3^{-/-}$ RT neurons compared to the wild-type (Figure 3). Similarly, in response to depolarizing inputs, a significant reduction in the number of intraburst spikes and in the frequency of subsequent tonic firing was observed in $Ca_V2.3^{-/-}$ neurons (Figure 6), suggesting that $Ca_V2.3$ channels contribute to excitability of those neurons. Potential influence of the AHP on the frequency of the subsequent tonic firing has been excluded by finding no statistically significant correlation between the amplitude of the preceding AHP and the frequency of the subsequent tonic firing, supporting our interpretation (data not shown). Moreover, an application of apamin to wild-type RT neurons in the presence of TTX unmasked a slowly decaying plateau potential (Cueni et al., 2008). The nonselective calcium-activated cationic current permeating Na^+, K^+, and Ca^{2+} (Luzhkov and Aqvist, 2001) could be a possible candidate of the long-lasting plateau potential that

was profoundly reduced in $Ca_V2.3^{-/-}$ neurons, suggesting that an initial LT Ca^{2+} influx further recruits $Ca_V2.3$ channels, which ensure the prolonged depolarization needed for increased firing activity of RT neurons. A similar role for $Ca_V2.3$ channels was also noted in the hyperexcitability induced by apamin (Figure S2).

Physiological Role of $Ca_V2.3$ Channels in Absence Seizures

Cellular and circuit properties of thalamic neurons give rise to thalamocortical oscillations in arousal/sleep states as well as seizures. RT neurons are known for their propensity to generate rhythmic burst discharges (Fuentealba and Steriade, 2005). It has been proposed that rhythmic burst discharges of RT neurons mediate inhibitory postsynaptic potentials in thalamocortical cells through $GABA_A$ and $GABA_B$ receptors (Kim et al., 1997). The $GABA_B$ receptor-mediated opening of K^+ channels induces rebound bursting in a large proportion of thalamocortical neurons, leading to a paroxysmal activity (Beenhakker and Huguenard, 2009; Crunelli and Leresche, 1991; Steriade et al., 1993; von Krosigk et al., 1993).

Systemic administration of the $GABA_B$ receptor agonist GBL induces experimental absence seizures in rodents (Ishige et al., 1996). Our results demonstrated that the lack of $Ca_V2.3$ channels in mice resulted in a marked decrement in the duration and power of GBL-induced 3–4 Hz SWDs, the hallmark of absence seizures. A pharmacological blockade of $Ca_V2.3$ channels in the RT also reduced the susceptibility of the mouse to GBL-induced 3–4 Hz SWDs, consistent with the results with the $Ca_V2.3^{-/-}$ mice. These results are consistent with a previous report that revealed a close correlation between SWDs on EEGs and rhythmic burst discharges of RT neurons on intracellular recordings observed in the genetic absence epileptic rat from Strasbourg (GAERS) model animals (Slaght et al., 2002). Correspondingly, the preservation of rhythms in a deafferented RT leads Steriade et al. (1987) to propose that the RT is the generator of rhythmicity during EEG synchronizations. Our results in vitro as well as in vivo using genetic and pharmacological tools suggest that $Ca_V2.3$ channels are critical for the rhythmic burst discharges of RT neurons that in turn may maintain thalamocortical rhythms (Llinas and Steriade, 2006; Steriade et al., 1993).

On the other hand, we note that the tonic firing activity of the RT neurons is reduced in the mutant, as shown by the reduced responses to depolarizing inputs (Figure 6). Therefore, it is formally feasible to suppose that the reduced excitability of the thalamocortical network rendered by the mutation contributes to the decreased sensitivity of the mutant mice to GBL-induced seizure responses.

Absence seizures are associated with EEG recordings of bilaterally synchronous SWDs. Here, we obtained simultaneous recordings of monopolar (Kim et al., 2001) and bipolar (subtraction method) EEGs (Weiergraber et al., 2008) in parallel from the same mice. However, only the monopolar data were included in the analysis because only this method of EEG recording yielded bilaterally synchronous SWDs with robust amplitudes, whereas bipolar recordings did not (~10-fold smaller), probably due to cancellation of the hemispherically symmetrical signals inherent to absence seizures (Figure S6). For this reason our findings may not be directly comparable to the bipolar EEG data previously reported for $Ca_V2.3^{-/-}$ mice (Weiergraber et al., 2008).

Future Perspectives

Patch-clamp and EEG recordings provide compelling evidence that $Ca_V2.3$ channels play a key role in the generation of rhythmic burst discharges of RT neurons and thalamocortical oscillations related to absence seizures. Moreover, it is known that LVA Ca^{2+} channels play an important role in absence seizures and sleep-related oscillations of the thalamocortical network (Cheong et al., 2009; Cueni et al., 2008; Kim et al., 2001). Taken together, understanding the functional consequences of modulation of HVA as well as LVA (Shin, 2006; Shin et al., 2008) Ca^{2+} channels may lead to defining the role of each type in oscillatory impairments in absence seizures and sleep disturbances, and help develop therapeutic tools to control relevant disorders of the thalamocortical network.

EXPERIMENTAL PROCEDURES

Animals

The $Ca_V2.3$ knockout mouse line (Lee et al., 2002) was mated with transgenic line, expressing green fluorescent protein (GFP) under GAD65 promoter (Lopez-Bendito et al., 2004). The $Ca_V2.3^{+/-}$/GAD65GFP$^{tg/+}$ mice were maintained in 129S4/SvJae as well as C57BL/6 genetic backgrounds and were mated to derive F1 progeny: B6129$Ca_V2.3^{+/+}$/GAD65GFP^{tg}, B6129$Ca_V2.3^{+/-}$/GAD65GFP^{tg}, and B6129$Ca_V2.3^{-/-}$/GAD65GFP^{tg}. For details see Supplemental Experimental Procedures.

Brain Slice Preparation

The mice at postnatal age 18–23 days were anesthetized with 150–200 μl of 2 bromo-2-Chloro-1,1,1-Trifluoroethane (Sigma-Aldrich; catalog No. b43888-250 ML). The brain was quickly removed and sectioned in the coronal plane, in carbogen-equilibrated ice-cold slicing solution containing 2.5 mM KCl, 10 mM $MgSO_4$, 1.25 mM NaH_2PO_4, 24 mM $NaHCO_3$, 0.5 mM $CaCl_2$-$2H_2O$, 11 mM glucose, and 234 mM sucrose. From rostral to caudal, 250 μm thick brain slices containing RT region were cut using a vibrating tissue slicer and were incubated in solution containing 124 mM NaCl, 3 mM KCl, 3 mM $MgSO_4$, 1.25 mM NaH_2PO_4, 26 mM $NaHCO_3$, 1 mM $CaCl_2$-$2H_2O$, and 10 mM glucose. Incubation was performed at 34°C for 1 hr before recording (Schofield et al., 2009).

Whole-Cell Patch Current-Clamp Recording

In K^+-based whole-cell current clamp mode, the intrinsic firing properties were recorded in coronal sections containing dorsal and lateral regions of RT, in recording solution of 124 mM NaCl, 3 mM KCl, 3 mM $MgSO_4$, 1.25 mM NaH_2PO_4, 26 mM $NaHCO_3$, 2.4 mM $CaCl_2$-$2H_2O$, and 10 mM glucose bubbled with 95% O_2/5% CO_2 at room temperature (23°C–25°C). For synaptic isolation of RT neurons, kynurenic acid (4 mM) and picrotoxin (50 μM) were included in control experiments. RT and individual neurons, expressing GFP marker under GAD65 promoter, were visualized through an upright epifluorescence microscope with a low-power objective (10×) and a high-power water-immersion objective (60×), and emitted fluorescence was detected through a Hamamatsu camera. Recording electrodes were pulled from fabricated standard-wall borosilicate glass capillary tubing (G150F-4: OD, 1.50 mm; ID, 0.86 mm; Warner Instruments) and had 4–6 MΩ tip resistance when filled with an intracellular solution containing140 mM K-gluconate, 10 mM KCl, 1 mM $MgCl_2$, 10 mM HEPES, 0.02 mM EGTA, 3 mM Mg-ATP, and 0.5 mM Na-GTP ([pH 7.35] 290–300 mosmol/l).

Whole-Cell Patch Voltage-Clamp Recording

Recordings for Ca^{2+} currents were performed at room temperature in an extracellular solution, as described previously (Sun et al., 2002), consisting of the following: 120 mM NaCl, 20 mM tetraethyl ammonium (TEA)-Cl, 2.5 mM

$CaCl_2$-$2H_2O$, 5 mM CsCl, 3 mM KCl, 10 mM HEPES, 2 mM $MgCl_2$, 1 mM 4-amino pyridine (4-AP), and 0.001 mM TTX. Patch pipettes were filled with cesium-based internal solution containing 117 mM Cs-gluconate, 13 mM KCl, 10 mM HEPES, 10 mM TEA-Cl, 10 mM BAPTA, 1 mM $MgCl_2$, 0.07 mM $CaCl_2$-$2H_2O$, 4 mM Mg-ATP, and 0.3 Na-GTP; pH was adjusted to 7.35 with CsOH, while osmolarity was adjusted to 290–300 mosmol/l with sucrose. For the recordings of SK_2 currents, extracellular as well as intracellular solutions were similar to those used for intrinsic firing properties except 1 mM TTX that was supplemented to the extracellular solution to block Na^+ currents. SK_2 currents were blocked by the application of 100 nM apamin. Neurons with Cm 45–60 pF with an access resistance of 10–20 MΩ were considered for recording. Access resistance was monitored before and after the experiment, and cells with an increase of the resistance by over 20% were excluded from the analysis. The currents were corrected for capacitive and leak currents using P/4 leak subtraction protocol. Signals were amplified with a Multiclamp700-A amplifier (Molecular Devices) and analyzed using pClamp10 (Axon Instruments, Foster City, CA, USA).

SNX-482 Injection to RT In Vivo

In 12- to 16-week-old F1(B6x129)$Ca_V2.3^{+/+}$/GAD65GFP^{tg} mice, a volume of 0.4 μl vehicle (0.9% NaCl) or SNX-482 (10 μM) was delivered at a rate of 0.1 μl/min through a 26G guide bilateral cannula (Plastics One) into the rostral as well as caudal RT (anteroposterior: −0.82 and −1.82 mm; lateral: −1.56 and −2.2 mm; ventral: 3.4 and 3.4 mm, respectively). For details see Supplemental Experimental Procedures.

EEG Electrode Implantation

Epidural electrodes were implanted bilaterally using a stereotaxic device (David Kopf Instruments) to the following coordinates with reference to bregma: anteroposterior, −0.8, +1.3, −1 mm; lateral, ±2, ±1.3, ±2.5 mm in young (Song et al., 2004), drug-injected (Cheong et al., 2009), and 16-week-old adult mice (Weiergraber et al., 2008), respectively. Ground electrode was implanted in the occipital region of brain (Schridde and Van Luijtelaar, 2004). Animals were given 7 days to fully recover before experiments (Kramer and Kinter, 2003). For comparison, real-time monopolar (Kim et al., 2001) and bipolar EEG (Weiergraber et al., 2008) recordings were performed at the age of ~16 weeks (Figure S6).

EEG Recording and Analysis

We recorded EEG signals using monopolar and bipolar methods in real time (sampling frequency, 10k Hz) in all groups. EEG activity was recorded for 1 hr using a pClamp10. SWDs separated by >1 s considered as separate event with voltage amplitude of twice the background EEG and a minimum duration of 0.7 s as described previously (Song et al., 2004). pClamp10 and MATLAB were utilized to detect SWDs based on amplitudes, peak-to-peak period, and shape from EEG signals filtered with a second-order Butterworth infinite impulse response (IIR), high-pass filter with a 2 Hz cutoff frequency.

Drugs

During slice recording the following drugs were used: SNX-482 (Louisville, KY, USA); apamin (Sigma- Aldrich); TTX (Tocris, Ballwin, MO, USA); TEA-Cl (GFS Chemicals, Columbus, OH, USA); and nifedipine, kynurenic acid, picrotoxin, and 4-AP (Sigma-Aldrich). For details on drugs see Supplemental Experimental Procedures.

Statistical Analysis

Data acquisition and analyses were performed using a combination of pClamp10, the Sigma Plot 9 integrated with Sigma Stat 3.1 (Jandel Scientific, San Rafael, CA, USA), and the Statistical Package for the Social Sciences version 14 (SPSS). Student's two-tailed t tests were used for comparisons. Two-way repeated ANOVA was carried out for EEG comparison between groups and within groups. All data are presented as mean ± SEM unless stated otherwise. p values of <0.05 were considered statistically significant.

SUPPLEMENTAL INFORMATION

Supplemental Information includes Supplemental Experimental Procedures, six figures, and one table and can be found with this article online at doi:10.1016/j.neuron.2011.02.042.

ACKNOWLEDGMENTS

We thank Chanki Kim, M.A. Aslam, Gireesh G., Sungsoo Jang, Soojung Lee, Il-hwan Choe, and Seung-eun Lee for technical as well as intellectual support. This work was supported by the National Honor Scientist Program of the Korean Government, and the WCI program of Korea Institute of Science and Technology.

Accepted: January 21, 2011
Published: April 13, 2011

REFERENCES

Avanzini, G., de Curtis, M., Panzica, F., and Spreafico, R. (1989). Intrinsic properties of nucleus reticularis thalami neurones of the rat studied in vitro. J. Physiol. *416*, 111–122.

Beenhakker, M.P., and Huguenard, J.R. (2009). Neurons that fire together also conspire together: is normal sleep circuitry hijacked to generate epilepsy? Neuron *62*, 612–632.

Blethyn, K.L., Hughes, S.W., Toth, T.I., Cope, D.W., and Crunelli, V. (2006). Neuronal basis of the slow (<1 Hz) oscillation in neurons of the nucleus reticularis thalami in vitro. J. Neurosci. *26*, 2474–2486.

Bourinet, E., Stotz, S.C., Spaetgens, R.L., Dayanithi, G., Lemos, J., Nargeot, J., and Zamponi, G.W. (2001). Interaction of SNX482 with domains III and IV inhibits activation gating of alpha(1E) (Ca(V)2.3) calcium channels. Biophys. J. *81*, 79–88.

Brenowitz, S.D., and Regehr, W.G. (2003). "Resistant" channels reluctantly reveal their roles. Neuron *39*, 391–394.

Breustedt, J., Vogt, K.E., Miller, R.J., Nicoll, R.A., Schmitz, D., Dietrich, D., Kirschstein, T., Kukley, M., Pereverzev, A., von der Brelie, C., et al. (2003). Alpha1E-containing Ca^{2+} channels are involved in synaptic plasticity. Proc. Natl. Acad. Sci. USA *100*, 12450–12455.

Cheong, E., Zheng, Y., Lee, K., Lee, J., Kim, S., Sanati, M., Lee, S., Kim, Y.S., and Shin, H.S. (2009). Deletion of phospholipase C beta4 in thalamocortical relay nucleus leads to absence seizures. Proc. Natl. Acad. Sci. USA *106*, 21912–21917.

Cloues, R.K., and Sather, W.A. (2003). Afterhyperpolarization regulates firing rate in neurons of the suprachiasmatic nucleus. J. Neurosci. *23*, 1593–1604.

Coleman, K.A., and Mitrofanis, J. (1996). Organization of the visual reticular thalamic nucleus of the rat. Eur. J. Neurosci. *8*, 388–404.

Crunelli, V., and Leresche, N. (1991). A role for GABAB receptors in excitation and inhibition of thalamocortical cells. Trends Neurosci. *14*, 16–21.

Cueni, L., Canepari, M., Lujan, R., Emmenegger, Y., Watanabe, M., Bond, C.T., Franken, P., Adelman, J.P., and Luthi, A. (2008). T-type Ca^{2+} channels, SK_2 channels and SERCAs gate sleep-related oscillations in thalamic dendrites. Nat. Neurosci. *11*, 683–692.

Debarbieux, F., Brunton, J., and Charpak, S. (1998). Effect of bicuculline on thalamic activity: a direct blockade of IAHP in reticularis neurons. J. Neurophysiol. *79*, 2911–2918.

Dietrich, D., Kirschstein, T., Kukley, M., Pereverzev, A., von der Brelie, C., Schneider, T., and Beck, H. (2003). Functional specialization of presynaptic Cav2.3 Ca^{2+} channels. Neuron *39*, 483–496.

Fox, A.P., Nowycky, M.C., and Tsien, R.W. (1987). Kinetic and pharmacological properties distinguishing three types of calcium currents in chick sensory neurones. J. Physiol. *394*, 149–172.

Fuentealba, P., and Steriade, M. (2005). The reticular nucleus revisited: intrinsic and network properties of a thalamic pacemaker. Prog. Neurobiol. *75*, 125–141.

Hu, R.Q., Cortez, M.A., Man, H.Y., Roder, J., Jia, Z., Wang, Y.T., and Snead, O.C., 3rd. (2001). Gamma-hydroxybutyric acid-induced absence seizures in GluR2 null mutant mice. Brain Res. *897*, 27–35.

Huguenard, J.R. (1996). Low-threshold calcium currents in central nervous system neurons. Annu. Rev. Physiol. *58*, 329–348.

Huguenard, J.R., and Prince, D.A. (1992). A novel T-type current underlies prolonged Ca^{2+}-dependent burst firing in GABAergic neurons of rat thalamic reticular nucleus. J. Neurosci. *12*, 3804–3817.

Huguenard, J.R., and McCormick, D.A. (2007). Thalamic synchrony and dynamic regulation of global forebrain oscillations. Trends Neurosci. *30*, 350–356.

Ishige, K., Aizawa, M., Ito, Y., and Fukuda, H. (1996). gamma-Butyrolactone-induced absence-like seizures increase nuclear CRE- and AP-1 DNA-binding activities in mouse brain. Neuropharmacology *35*, 45–55.

Joksovic, P.M., Bayliss, D.A., and Todorovic, S.M. (2005). Different kinetic properties of two T-type Ca^{2+} currents of rat reticular thalamic neurones and their modulation by enflurane. J. Physiol. *566*, 125–142.

Joksovic, P.M., Weiergraber, M., Lee, W., Struck, H., Schneider, T., and Todorovic, S.M. (2009). Isoflurane-sensitive presynaptic R-type calcium channels contribute to inhibitory synaptic transmission in the rat thalamus. J. Neurosci. *29*, 1434–1445.

Jones, E.G. (1975). Some aspects of the organization of the thalamic reticular complex. J. Comp. Neurol. *162*, 285–308.

Kim, D., Song, I., Keum, S., Lee, T., Jeong, M.J., Kim, S.S., McEnery, M.W., and Shin, H.S. (2001). Lack of the burst firing of thalamocortical relay neurons and resistance to absence seizures in mice lacking alpha(1G) T-type Ca^{2+} channels. Neuron *31*, 35–45.

Kim, U., Sanchez-Vives, M.V., and McCormick, D.A. (1997). Functional dynamics of GABAergic inhibition in the thalamus. Science *278*, 130–134.

Kramer, K., and Kinter, L.B. (2003). Evaluation and applications of radiotelemetry in small laboratory animals. Physiol. Genomics *13*, 197–205.

Lee, S.C., Choi, S., Lee, T., Kim, H.L., Chin, H., and Shin, H.S. (2002). Molecular basis of R-type calcium channels in central amygdala neurons of the mouse. Proc. Natl. Acad. Sci. USA *99*, 3276–3281.

Lee, S.H., Govindaiah, G., and Cox, C.L. (2007). Heterogeneity of firing properties among rat thalamic reticular nucleus neurons. J. Physiol. *582*, 195–208.

Leroy, J., Pereverzev, A., Vajna, R., Qin, N., Pfitzer, G., Hescheler, J., Malecot, C.O., Schneider, T., and Klockner, U. (2003). Ca^{2+}-sensitive regulation of E-type Ca^{2+} channel activity depends on an arginine-rich region in the cytosolic II-III loop. Eur. J. Neurosci. *18*, 841–855.

Llinas, R.R. (1988). The intrinsic electrophysiological properties of mammalian neurons: insights into central nervous system function. Science *242*, 1654–1664.

Llinas, R.R., and Steriade, M. (2006). Bursting of thalamic neurons and states of vigilance. J. Neurophysiol. *95*, 3297–3308.

Lopez-Bendito, G., Sturgess, K., Erdelyi, F., Szabo, G., Molnar, Z., and Paulsen, O. (2004). Preferential origin and layer destination of GAD65-GFP cortical interneurons. Cereb. Cortex *14*, 1122–1133.

Luzhkov, V.B., and Aqvist, J. (2001). K(+)/Na(+) selectivity of the KcsA potassium channel from microscopic free energy perturbation calculations. Biochim. Biophys. Acta *1548*, 194–202.

Newcomb, R., Szoke, B., Palma, A., Wang, G., Chen, X., Hopkins, W., Cong, R., Miller, J., Urge, L., Tarczy-Hornoch, K., et al. (1998). Selective peptide antagonist of the class E calcium channel from the venom of the tarantula *Hysterocrates gigas*. Biochemistry *37*, 15353–15362.

Newcomb, R., Chen, X.-h., Dean, R., Dayanithi, G., Cong, R., Szoke, B., Lemos, J., Bowersox, S., and Miljanich, G. (2000). SNX-482: a novel class E calcium channel antagonist from tarantula venom. CNS Drug Rev. *6*, 153–173.

Pape, H.C., Munsch, T., and Budde, T. (2004). Novel vistas of calcium-mediated signalling in the thalamus. Pflugers Arch. *448*, 131–138.

Pereverzev, A., Leroy, J., Krieger, A., Malecot, C.O., Hescheler, J., Pfitzer, G., Klockner, U., and Schneider, T. (2002). Alternate splicing in the cytosolic II-III loop and the carboxy terminus of human E-type voltage-gated Ca^{2+} channels: electrophysiological characterization of isoforms. Mol. Cell. Neurosci. *21*, 352–365.

Perez-Reyes, E. (2003). Molecular physiology of low-voltage-activated t-type calcium channels. Physiol. Rev. *83*, 117–161.

Randall, A.D., and Tsien, R.W. (1997). Contrasting biophysical and pharmacological properties of T-type and R-type calcium channels. Neuropharmacology *36*, 879–893.

Rhee, J.S., Ishibashi, H., and Akaike, N. (1999). Calcium channels in the GABAergic presynaptic nerve terminals projecting to meynert neurons of the rat. J. Neurochem. *72*, 800–807.

Saegusa, H., Kurihara, T., Zong, S., Minowa, O., Kazuno, A., Han, W., Matsuda, Y., Yamanaka, H., Osanai, M., Noda, T., and Tanabe, T. (2000). Altered pain responses in mice lacking alpha 1E subunit of the voltage-dependent Ca^{2+} channel. Proc. Natl. Acad. Sci. USA *97*, 6132–6137.

Sah, P. (1996). Ca^{2+}-activated K^+ currents in neurones: types, physiological roles and modulation. Trends Neurosci. *19*, 150–154.

Sah, P., and McLachlan, E.M. (1991). Ca^{2+}-activated K^+ currents underlying the afterhyperpolarization in guinea pig vagal neurons: a role for Ca^{2+}-activated Ca^{2+} release. Neuron *7*, 257–264.

Schofield, C.M., Kleiman-Weiner, M., Rudolph, U., and Huguenard, J.R. (2009). A gain in GABAA receptor synaptic strength in thalamus reduces oscillatory activity and absence seizures. Proc. Natl. Acad. Sci. USA *106*, 7630–7635.

Schridde, U., and Van Luijtelaar, E.L. (2004). The influence of strain and housing on two types of spike-wave discharges in rats. Genes Brain Behav. *3*, 1–7.

Shin, H.S. (2006). T-type Ca^{2+} channels and absence epilepsy. Cell Calcium *40*, 191–196.

Shin, H.S., Cheong, E.J., Choi, S., Lee, J., and Na, H.S. (2008). T-type Ca^{2+} channels as therapeutic targets in the nervous system. Curr. Opin. Pharmacol. *8*, 33–41.

Slaght, S.J., Leresche, N., Deniau, J.M., Crunelli, V., and Charpier, S. (2002). Activity of thalamic reticular neurons during spontaneous genetically determined spike and wave discharges. J. Neurosci. *22*, 2323–2334.

Snead, O.C., 3rd. (1988). gamma-Hydroxybutyrate model of generalized absence seizures: further characterization and comparison with other absence models. Epilepsia *29*, 361–368.

Song, I., Kim, D., Choi, S., Sun, M., Kim, Y., and Shin, H.S. (2004). Role of the alpha1G T-type calcium channel in spontaneous absence seizures in mutant mice. J. Neurosci. *24*, 5249–5257.

Soong, T.W., Stea, A., Hodson, C.D., Dubel, S.J., Vincent, S.R., and Snutch, T.P. (1993). Structure and functional expression of a member of the low voltage-activated calcium channel family. Science *260*, 1133–1136.

Steriade, M. (2006). Grouping of brain rhythms in corticothalamic systems. Neuroscience *137*, 1087–1106.

Steriade, M., Domich, L., and Oakson, G. (1986). Reticularis thalami neurons revisited: activity changes during shifts in states of vigilance. J. Neurosci. *6*, 68–81.

Steriade, M., Domich, L., Oakson, G., and Deschenes, M. (1987). The deafferented reticular thalamic nucleus generates spindle rhythmicity. J. Neurophysiol. *57*, 260–273.

Steriade, M., McCormick, D.A., and Sejnowski, T.J. (1993). Thalamocortical oscillations in the sleeping and aroused brain. Science *262*, 679–685.

Sun, Q.Q., Huguenard, J.R., and Prince, D.A. (2002). Somatostatin inhibits thalamic network oscillations in vitro: actions on the GABAergic neurons of the reticular nucleus. J. Neurosci. *22*, 5374–5386.

Takahashi, T., and Momiyama, A. (1993). Different types of calcium channels mediate central synaptic transmission. Nature *366*, 156–158.

Tottene, A., Volsen, S., and Pietrobon, D. (2000). alpha(1E) subunits form the pore of three cerebellar R-type calcium channels with different pharmacological and permeation properties. J. Neurosci. *20*, 171–178.

von Krosigk, M., Bal, T., and McCormick, D.A. (1993). Cellular mechanisms of a synchronized oscillation in the thalamus. Science *261*, 361–364.

Weiergraber, M., Kamp, M.A., Radhakrishnan, K., Hescheler, J., and Schneider, T. (2006). The Ca(v)2.3 voltage-gated calcium channel in epileptogenesis–shedding new light on an enigmatic channel. Neurosci. Biobehav. Rev. *30*, 1122–1144.

Weiergraber, M., Henry, M., Ho, M.S., Struck, H., Hescheler, J., and Schneider, T. (2008). Altered thalamocortical rhythmicity in Ca(v)2.3-deficient mice. Mol. Cell. Neurosci. *39*, 605–618.

Yazdi, H.H., Janahmadi, M., and Behzadi, G. (2007). The role of small-conductance Ca^{2+}-activated K^+ channels in the modulation of 4-aminopyridine-induced burst firing in rat cerebellar Purkinje cells. Brain Res. *1156*, 59–66.

Zamponi, G.W., Bourinet, E., and Snutch, T.P. (1996). Nickel block of a family of neuronal calcium channels: subtype- and subunit-dependent action at multiple sites. J. Membr. Biol. *151*, 77–90.